

Article

# Effect of Induction Heating on Surface Properties of Hot-Pressed Ceramics Based on Nanopowders $\text{Si}_3\text{N}_4$ and TiN

Lina L. Sartinska 

Frantsevich Institute for Problems of Materials Science of NAS of Ukraine, 3 Krzhyzhanovsky Str., 03142 Kiev, Ukraine; sart@ipms.kiev.ua; Tel.: +380-(0)-67-592-10-52

**Abstract:** The effect of induction heating on the surface properties of hot-pressed ceramics based on plasma chemical nanopowders  $\text{Si}_3\text{N}_4$  and TiN (additives:  $\text{Al}_2\text{O}_3$ , AlN, and  $\text{Y}_2\text{O}_3$ ) has been studied. The research demonstrates the formation of a modified layer on the surface of the hot-pressed material. The study examines the porosity, hardness, fracture toughness, brittleness, distribution of elements, and wear of hot-pressed ceramics on the surface before and after additional grinding. Removal of the surface porous layer results in increased density and hardness, leading to a higher number of acoustic emission signals during scratching with a Vickers indenter. A different response to scratching indicates a transgranular or intergranular fracture of the structure. The presence of porosity and carbon contamination on the surface layer of materials negatively impacts the properties of TiN-reinforced ceramics based on  $\text{Si}_3\text{N}_4$ - $\text{Al}_2\text{O}_3$ -AlN (SIALON). However, the addition of  $\text{Y}_2\text{O}_3$  effectively prevents carbon penetration and reduces the effect of grinding. Additionally, the dark-colored tone observed on the outer volume of the samples suggests a non-thermal microwave effect of the induction furnace.

**Keywords:** nitrides; plasma chemical nanopowders; hot-pressing; surface properties; mechanical properties; wear; grinding; non-thermal microwave effect



**Citation:** Sartinska, L.L. Effect of Induction Heating on Surface Properties of Hot-Pressed Ceramics Based on Nanopowders  $\text{Si}_3\text{N}_4$  and TiN. *Powders* **2023**, *2*, 697–708. <https://doi.org/10.3390/powders2040043>

Academic Editor: Paul F. Luckham

Received: 20 June 2023

Revised: 6 August 2023

Accepted: 10 October 2023

Published: 18 October 2023



**Copyright:** © 2023 by the author. Licensee MDPI, Basel, Switzerland. This article is an open access article distributed under the terms and conditions of the Creative Commons Attribution (CC BY) license (<https://creativecommons.org/licenses/by/4.0/>).

## 1. Introduction

Ceramics based on nanopowders can exhibit prominent properties since these powders display different and usually outstanding physical and chemical properties as compared to their larger counterparts. For example, ceramics based on silicon nitride ( $\text{Si}_3\text{N}_4$ ) nanopowders can exhibit plastic behavior even if they are typically tough and strong [1]. Nanoparticles of  $\text{Si}_3\text{N}_4$  are also indispensable components for the next generation of high-power electronic devices and for the fabrication of electronic devices operating at high temperatures and high frequencies in harsh environments [2–4]. Structural applications such as automotive engine parts, heat exchangers, pump seal parts, ball bearings, cutting tools, and ceramic armor, due to its low bulk density, excellent mechanical properties at elevated temperatures, high resistance to thermal shock and chemical attack, excellent creep resistance, and good tribological and wear properties, are also features of these  $\text{Si}_3\text{N}_4$  ceramics [5,6]. The use of a reduced particle size of  $\text{Si}_3\text{N}_4$ , which improves sinterability, will overcome limitations caused by factors such as the strong covalent structure of  $\text{Si}_3\text{N}_4$ , which requires high sintering temperatures, thereby increasing processing costs [7].

It is known that the composition of  $\text{Si}_3\text{N}_4$  ceramic materials can significantly affect their mechanical properties [5,8–10]. The amount of additive initially introduced to the ceramics determines the quantity and chemistry of its glass phase and changes properties such as fracture toughness, ambient and high temperature strengths, creep resistance, and oxidation resistance [11–14]. There is a direct connection between microstructure, namely the grain growth of nanopowders, grain boundary chemistry, and mechanical behaviors of silicon nitride ceramics [15–18]. A coarse structure, as a rule, results from the accelerated diffusion of atoms in the liquid phase at high temperatures. [19]. A variety

of combinations of additives and their appropriate amounts in preparing  $\text{Si}_3\text{N}_4$  ceramics based on nanopowders are essential for attaining full densification and achieving their high-performance properties [5,20–22].

The microstructure of ceramics strongly depends on the processing [5,7,9,20–26]. Pressure sintering can result in a higher density of ceramic materials compared to pressureless sintering [15,27,28]. The orientation of nanostructures determined by heat flux, testing temperature, and the  $\alpha/\beta$   $\text{Si}_3\text{N}_4$  phase ratio provides a less resistive network and the intrinsic anisotropy of thermal conductivity in the in-plane direction of the heat flux [15,29,30]. High fracture resistance combined with a steeply rising R-curve and high fracture strength can be developed in self-reinforced silicon nitrides by careful control of the size and amount of well-dispersed large elongated grains in a fine-grained matrix. If not regulated, a microstructure with a broad grain diameter distribution tends to form. A significant reduction in strength is observed when microstructures consisting of a broad grain diameter distribution are generated. When a finely equiaxed microstructure is generated, both the fracture strength and the fracture resistance are reduced [31].

It is known that such principal parameters as strength, hardness, fracture toughness, and wear resistance are frequently uncorrelated with each other, and very often, researchers working in the field of ceramics have failed to match the level of their mechanical properties. One of the reasons for this occurrence is the formation of gradient structures and the existence of a modified layer on the surface of the prepared ceramics [32]. Phase compositions, microstructures, mechanical properties, and wear behaviors were investigated. The main  $\alpha$ - $\text{Si}_3\text{N}_4$  phase was detected in the outer layers, and only  $\beta$ - $\text{Si}_3\text{N}_4$  phase was observed in the inner layers. The Vickers hardness of the outer layer was much higher than that of the inner layer, whereas the fracture toughness of the outer layer was much lower than that of the inner layer, indicative of the hard surface and tough core. The graded  $\text{Si}_3\text{N}_4$  ceramics exhibited superior wear resistance with a low wear rate due to the ultra-fine microstructure and high hardness of the outer layer [32].

A skin layer that was generated near the surface of hot-pressed silicon nitride ceramics was studied from a microscopic viewpoint. The ceramics were composed of acicular  $\beta$ - $\text{Si}_3\text{N}_4$  grains and a glassy grain boundary that was liquid at hot-pressing temperature. It was demonstrated that the thickness of the skin layer increased with an increase in the amount of sintering additive. A compositional difference in glassy phases was observed between the surface layer and the bulk of  $\text{Si}_3\text{N}_4$  ceramics [33].

Over the years, there has been growing evidence of the unusual effects of microwave or induction energy [22,27]. Microwave heating facilitates sintering and grain growth by decreasing the activation energy of diffusion, increasing ionic interdiffusion, and thereby promoting the formation of a gradient structure in the sintered material. The reason for its formation may be related to the difference between annealing and microwave [27,34]. Unexpected magnetism in dielectric oxide nanostructured materials, even at room temperature, can also be the reason for the formation of a gradient structure [35,36]. The unique magnetism of nanomaterials is usually associated with various structural defects, such as cation vacancies, oxygen vacancies, and structural inhomogeneity, which is confirmed by numerous studies of highly defective magnetic oxides and nitrides [36].

Thus, the main objective of this research is to fabricate materials based on nanopowders and study how the composition of the original nanopowders and sintering conditions influence the formation of a modified surface layer on ceramics. Additionally, the research aims to assess the impact of this modified layer on the material properties.

## 2. Materials and Methods

Silicon nitride ( $\text{Si}_3\text{N}_4$ ), titanium nitride (TiN), and alumina ( $\text{Al}_2\text{O}_3$ ) powders prepared by plasma chemical synthesis of mean size  $\leq 0.03 \mu\text{m}$  were used as initial powders [37,38]. As received, these powders were electrostatically charged and could shift under the effect of a magnetic field. After being in an open environment for two months, they have been losing this ability. It was discovered that one of the reasons for this phenomenon was an

increase in the adsorbed oxygen content from 1 wt. % up to 5 wt. % on the surface of this powder.

Yttrium oxide ( $Y_2O_3$ ) powder (mean size  $\leq 1.5 \mu\text{m}$ ) was also selected as a sintering additive.

Mixing weighed quantities of powders was carried out in a planetary ball mill for 20 min in an acetone medium [39]. The planetary mill had four cylinders, each with a volume of 250 mL. The mass of the loaded balls is 100 g for each cylinder; the acceleration of the grinding bodies is 6 g; and the mass of the material load to be processed is 20 g. Ceramic balls with a diameter of 3, 5, and 6 mm were used as the grinding bodies.

Hot pressing of plasma chemical powders was performed in multi-cavity graphite dies at a temperature of 1820 °C in air at a pressure of 20 MPa applied along one axis and at a dwell time of 1–8 min. The surfaces of graphite dies and punches were covered with boron nitride lubricant. The induction heating was done using high-frequency generators at 5.3 MHz. After sintering, the samples were cleaned, ground, and polished using a special machine (Figure 1). The apparent density of all dense samples was measured by a standard water immersion technique. The specimens were ground for making cutters ( $12.7 \times 12.7 \text{ mm}$ , thickness 4.76 mm, and  $6.35 \times 6.35 \text{ mm}$ , thickness 2.38 mm) [40–42] (Figure 1c).

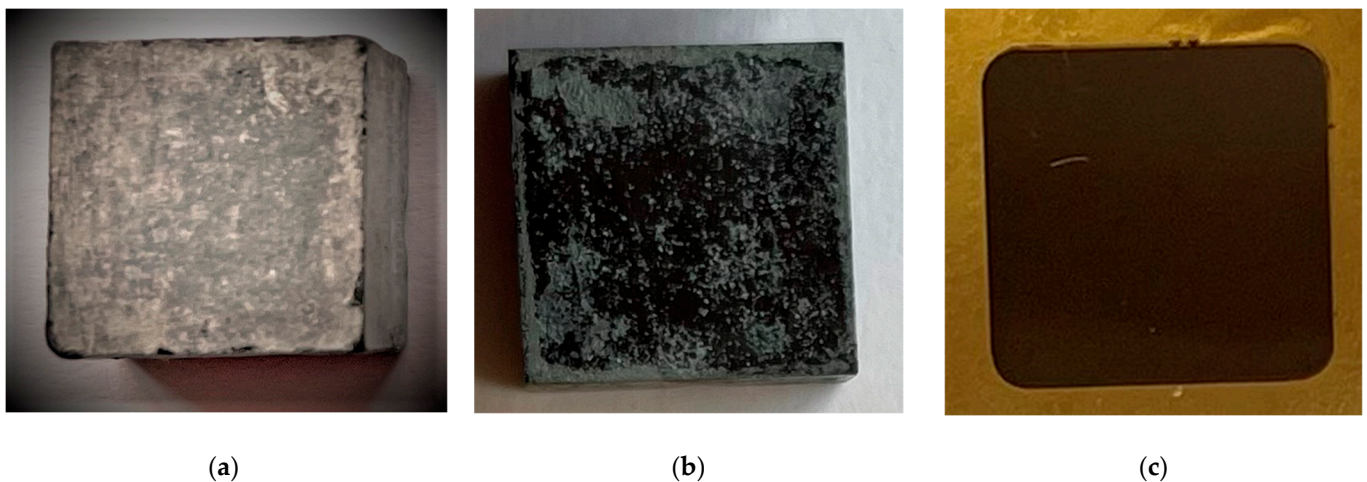


**Figure 1.** A general view photograph of the hot-pressed sample: (a)—as received; (b)—after cleaning for apparent density measurements; (c)—polished cutter ( $12.7 \times 12.7 \text{ mm}$ , thickness 4.76 mm) in epoxy resin.

The compositions and structures of ceramic materials based on plasma chemical powders were analyzed by an electron probe microanalyzer (Superprobe-733) [39,40].

Hardness and fracture toughness ( $K_{1c}$ ) were measured by a standard micro-indentation technique using a Vickers indenter with a square tip at a load of 50 N for 10 s. The determination of hardness was performed using the method of unrestored print.  $K_{1c}$  was calculated using the equation of Niihara [43]. The life tests of the cutters made of plasma-chemical powders were performed in turning hardened steels at speeds of 300 m/min, a feed of 0.1 mm/rev, and depths of 0.5 and 1.0 mm by determining the amount of dulling of the cutter on the flank ( $h_3$ ) in 15 min (the radius of curvature of the cutting tip was 0.3 mm) [39–42]. The measurement of the brittleness of the surface layers was made by the acoustic emission method in the process of scratching the surface with a Vickers indenter with a load of 10 N [44,45].

### 3. Results

#### 3.1. Density, Hardness, and Fracture Toughness Measurements

The results demonstrate that TiN-reinforced ceramics based on SIALON exhibit the highest density (Table 1, samples 12–17) and low porosity. Conversely, TiN-reinforced ce-

ramics based on  $\text{Si}_3\text{N}_4$ , prepared without a sintering additive, displayed the lowest density (Table 1, samples 18–19). However, the introduction of  $\text{Y}_2\text{O}_3$  as a sintering additive to these  $\text{Si}_3\text{N}_4$  powders significantly reduced their porosity (Table 1, samples 2–5). Additionally, the density of samples based on plasma chemical powders increased by approximately 2% after undergoing additional surface grinding. Given that the typical porosity of these materials ranged from 1% to 3% (Table 1), it can be concluded that the porosity of such hot-pressed ceramics is primarily localized on the surface.

**Table 1.** Composition and porosity of hot-pressed samples made of plasma chemical powders before and after additional grinding.

Samples	Composition, wt.%					Porosity, %	
	$\text{Si}_3\text{N}_4$	$\text{Al}_2\text{O}_3$	AlN	$\text{Y}_2\text{O}_3$	TiN	before Grinding	after Additional Grinding
1	95			5		2.0	1.8
2	55.4			5	39.6	2.2	1.6
3	46.5			0.5	53	3.2	3.0
4	27			5	68	3.9	3.7
5	27.5			2.5	70	3.1	3.0
6	61.2	22.3		16.5		1.6	1.1
7	75	2		3	20	2.8	2.0
8		25	35		40	2.3	1.2
9		14	38		48	2.0	1.7
10			50		50	4.1	3.9
11		50			50	2.4	2.2
12	27	19	24		30	1.9	1.0
13	56	12	2		30	1.0	0.1
14	21	26	53		40	0.8	0.2
15	12.6	15.6	31.7		40	1.1	0.8
16	36.6	15.4	6.2		41.8	0.8	0.1
17	35	25	10		30	1.7	0.6
18	87.7				12.3	12.4	12.4
19	50				50	6.1	6.0

Hardness is a property that indirectly reveals the mechanical strength of ceramics. It is determined by the material's resistance to brittle fracture rather than plastic deformation. As a result, hardness can be indicative of the material's crack resistance. The extent to which the fracture process influences hardness changes with the applied load and depends on the nature, type, and size of the formed cracks in the fracture zone (Figure 2). The indentation test is commonly employed to determine the ceramics' resistance against crack initiation and propagation. The development and dimensions of the cracks provide insights into both the mechanical hardness and fracture toughness of the ceramic material. At low indentation loads, a deformed region forms beneath and near the indentation, leading to the emergence of four cracks emanating from the vertices of the square indentation (Figure 2a). On the other hand, using relatively large loads often results in the destruction of brittle ceramic materials within the indentation zone (Figure 2b).

The hardness of hot-pressed ceramic material composed of  $\text{Al}_2\text{O}_3$ -AlN-TiN (Table 1, sample 8) increases with an increasing load up to 100 N but then decreases as the load further increases to 500 N. This observed dependence contradicts the nonlinear relationship between hardness and loads reported in [46,47], where the highest hardness at 100 N is not

present. The occurrence of the highest hardness at 100 N may be attributed to the unique nanostructure features of ceramics based on plasma chemical powders. However, as the load continues to increase, the material undergoes destruction, leading to a decrease in hardness, similar to what has been observed in [46,47].

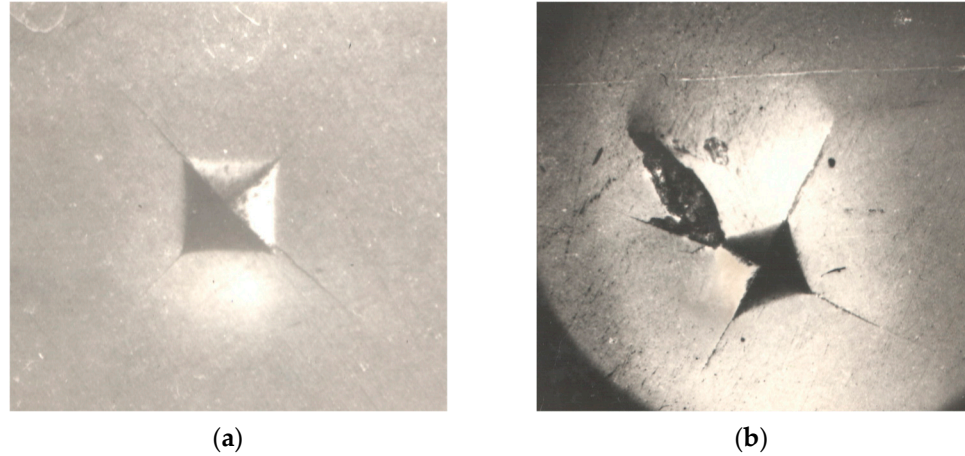


**Figure 2.** Vickers hardness impressions on hot-pressed ceramic material composed  $Al_2O_3$ -AlN-TiN at the loads: (a)—50 N; (b)—500 N.

Additional surface grinding results in an overall hardness increase of 20%, and the dependence on the load (50–500 N) remains relatively unchanged (Figure 3a).

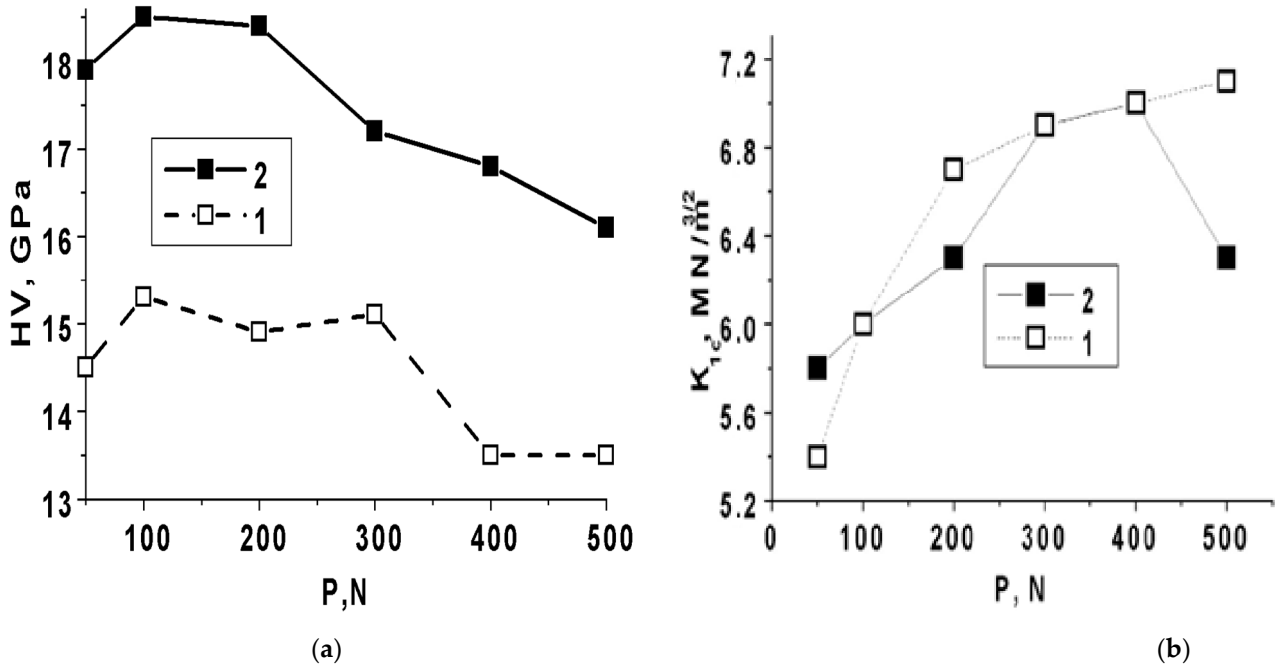


**Figure 3.** Hardness (a) and fracture toughness (b) of ceramic material composed of  $Al_2O_3$ -AlN-TiN (Table 1, sample 8) vs. load: 1—before; 2—after additional grinding.

Without additional grinding, the fracture toughness of ceramics composed of  $Al_2O_3$ -AlN-TiN increases with an increasing load up to 500 N (Figure 3b). This contrasts with the dependence observed in [46] for hard metals. This difference can be explained by the quenching effect on crack propagation within the pores of the surface layer. However, after additional grinding, the increasing trend of fracture toughness with an increasing load up to 500 N becomes less pronounced, and the data exhibits greater scatter (Figure 3b).

This phenomenon can be attributed to the uneven distribution of residual porosity and deformation stresses within the nanostructure of the material.

### 3.2. Acoustic Emission Signals Measurements

Measurements of acoustic emission signals or transient mechanical waves spontaneously generated by abrupt localized changes of strain within a material have shown that acoustic emission contains information about the characteristics of the material. Higher-density materials generate more acoustic emission signals as dislocation motion increases and cracks grow, which are the main mechanisms of strain change when materials are scratched.

Measurements of brittleness by acoustic emission on the surface of ceramic composites made of plasma chemical powders (Table 1) showed that in the process of scratching the surface with a Vickers indenter (load of 10 N), the number of acoustic emission signals increases sharply for most examined materials after additional grinding (Table 2, samples 6–9). Only for materials of high porosity (>12.4%), the number of acoustic emission signals does not change after grinding.

**Table 2.** Properties of the hot-pressed ceramic composites made of plasma chemical powders without and after additional grinding.

Samples	Composition, %					Total Porosity %	Hardness HV GPa	Toughness $K_{1c}$ MPa·m <sup>1/2</sup>	Total Number of Acoustic Signals
	Si <sub>3</sub> N <sub>4</sub>	Al <sub>2</sub> O <sub>3</sub>	AlN	Y <sub>2</sub> O <sub>3</sub>	TiN				
<i>Without additional grinding</i>									
1	75	2		3	20	2.2	18.4	7	7
2	61.2	22.3		16.5		3.3	14.9	5.2	40
3	55.4			5	39.6	1.4	12.4	5.4	21
4	55.4			5	39.6	2.3	14.7	7	170
5	87.7				12.3	12.4	1.6	2.3	14
<i>After additional grinding</i>									
6	12.6	15.6	31.7		40	0	18.2	5.8	25,000
7	36.6	15.4	6.2		41.8	0	19.7	7.6	130,000
8	55.4			5	39.6	0.8	16	7.1	2700
9	36.6	15.4	6.2		41.8	2.9	17.8	5.4	20,000
10	87.7				12.3	12.4	1.6	2.3	14

The failure of ceramic materials is characterized by low toughness, which leads to brittle fracture without preceding plastic deformation, subcritical crack extension, and large scatter in the mechanical properties. However, there is a close relationship between the number of acoustic emission signals and the hardness and fracture toughness of ceramics (Table 2, samples 6, 7, and 9) since the failure of ceramics based on SiALON matrix reinforced with TiN occurs by the mechanism of transgranular fracture (Figure 4a) [39–42,48–52].

For composite ceramics based on the Si<sub>3</sub>N<sub>4</sub> matrix with 5 wt. % Y<sub>2</sub>O<sub>3</sub> reinforced with TiN (Table 2, sample 8), intergranular fracture occurs (Figure 4b). Intergranular fracture typically arises when the phase at the grain boundary is weak and brittle. Consequently, crack propagation occurs along the grain boundaries of Si<sub>3</sub>N<sub>4</sub> and TiN, leading to fractures that follow the grain pattern of the material. As cracks are initiated and propagate in a brittle material, they continue to grow and increase in size.

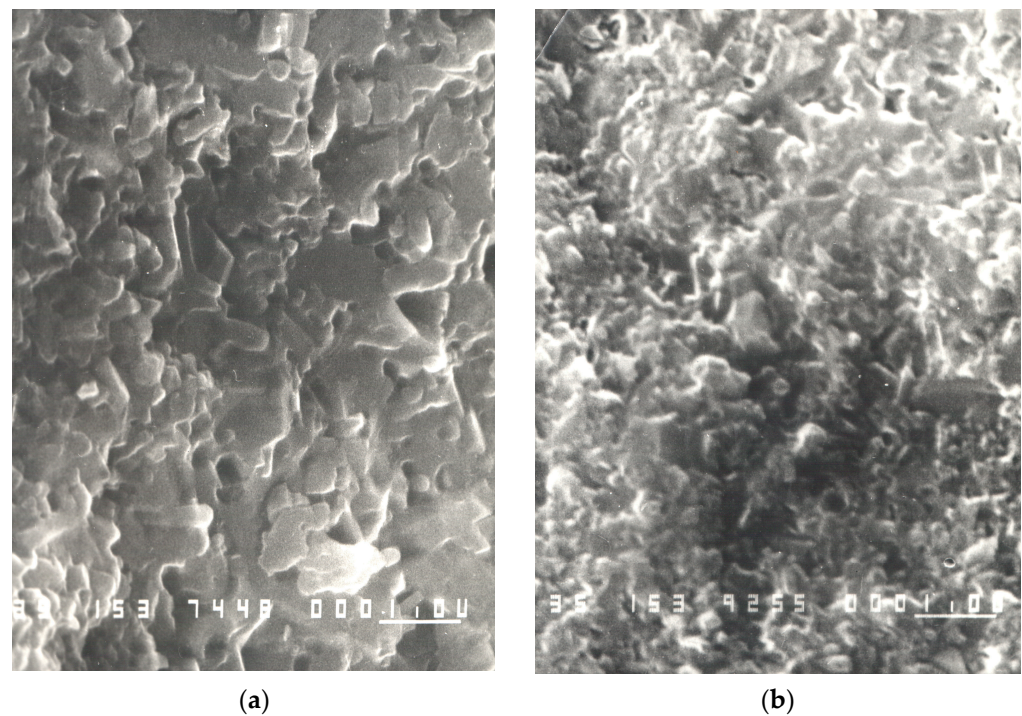


**Figure 4.** Micrographs of the transgranular (a) and intergranular (b) fracture of ceramics based on  $\text{Si}_3\text{N}_4$  and TiN.

The Vickers hardness of the composite ceramics based on the  $\text{Si}_3\text{N}_4$  matrix with 5 wt. %  $\text{Y}_2\text{O}_3$  reinforced with TiN (Table 2, sample 8) was found to be insufficiently high. However, the fracture toughness was high, comparable to the best ceramic sample based on the TiN-reinforced SIALON matrix with higher hardness (Table 2, sample 7). This phenomenon can be attributed to intergranular fracture, which leads to the formation of many small cracks with low energy release in a fine-grained structure. Considering the sensitivity of the device used for registering acoustic emission signals and the material's structure under investigation, the number of acoustic emission signals will be significantly lower. This is further supported by the results obtained for the sample of composite ceramics based on  $\text{Si}_3\text{N}_4$  matrix-reinforced TiN with 5 wt. %  $\text{Y}_2\text{O}_3$  (Table 2, sample 8).

### 3.3. Wear Measurements

All tested samples based on plasma chemical powders, as prepared, demonstrated a high level of wear (Figure 5, Table 1 (3–5, 9–11, 12–15)). The ceramic composite materials based on SIALON reinforced with TiN (Table 1, samples 12–15) exhibited the highest wear before grinding. This wear was caused by the presence of surface porosity and an increased carbon content on the sample's surface, as indicated by X-ray microanalysis (Figure 6). In contrast, X-ray microanalysis of samples based on  $\text{Si}_3\text{N}_4$ -  $\text{Y}_2\text{O}_3$ -TiN did not reveal the presence of carbon, even though all the studied samples were hot-pressed in the same graphite die. Consequently, the wear of these samples turned out to be two times lower (Table 1, samples 3–5). However, after grinding the surface layer off, the wear of all the studied ceramic composites decreased to 0.1 mm (Figure 5a).

A study was conducted on composite ceramic cutters ( $6.35 \times 6.35$  mm, thickness 2.38 mm) based on  $\text{Si}_3\text{N}_4$  reinforced with different percentages of TiN (ranging from 12.3% to 80%) along with 5 wt. %  $\text{Y}_2\text{O}_3$ , used for turning hardened steels at speeds of 300 m/min for 15 min (Figure 5b). The results indicated that having only 12.3 wt. % TiN in the cutter composition was insufficient to achieve the desired cutting ability under the current research conditions. On the other hand, including 80 wt. % TiN in the cutter composition led to high wear due to inadequate densification of the initial powders and resulting low cutter density. However, when the cutters were reinforced with TiN ranging from 23% to

70%, the wear remained constant and amounted to 0.1 mm during the turning of hardened steels at speeds of 300 m/min for 15 min (Figure 5b). This finding suggests that this range of TiN reinforcement was optimal for maintaining consistent cutting performance under the specified conditions.

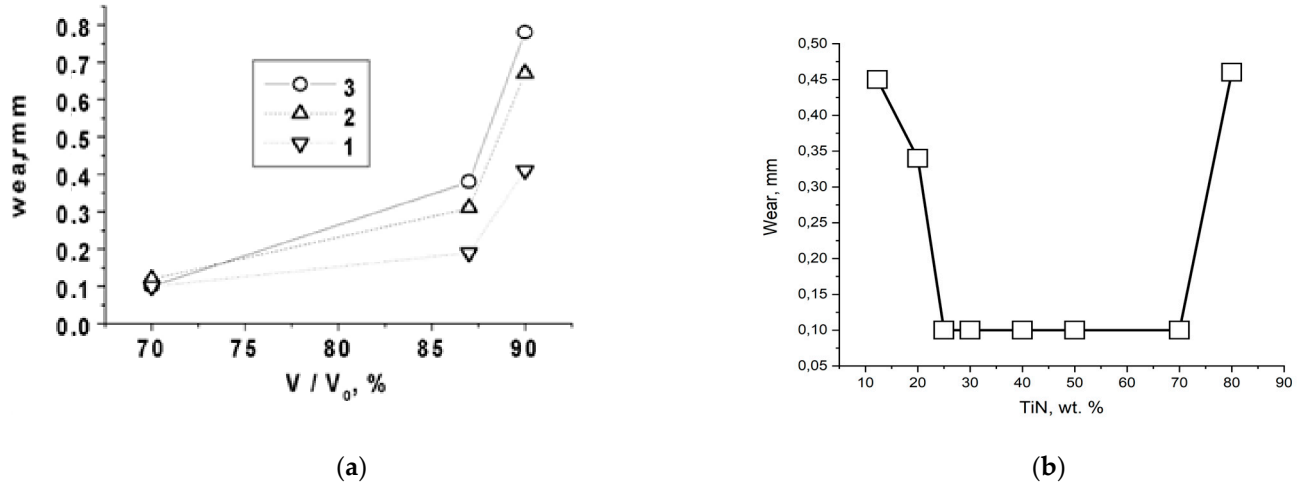


**Figure 5.** Wear vs. a sample relative volume (a) and TiN content (b). Composition of the samples (Table 1): 1-samples 3–5; 2-samples 8–9; 3-samples 12–15.

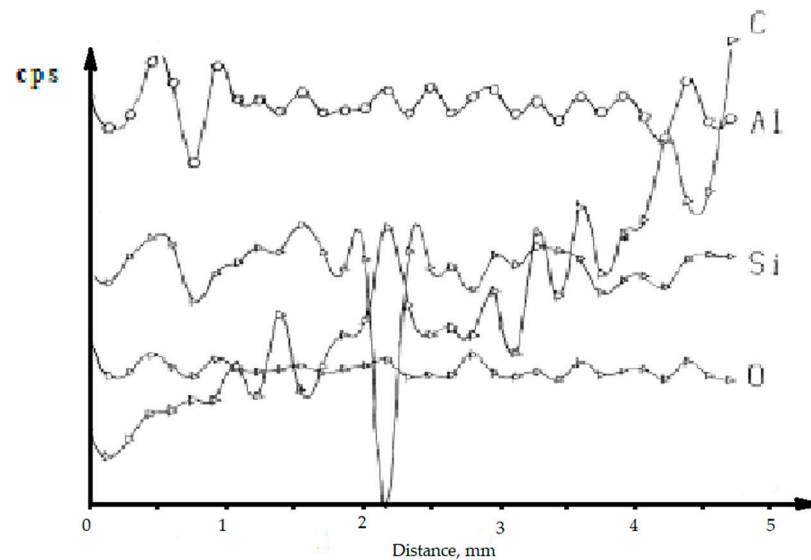


**Figure 6.** Emission intensity of different elements versus distance from the center of the sample to the edge of ceramics based on  $\text{Si}_3\text{N}_4\text{-Al}_2\text{O}_3\text{-AlN-TiN}$  (Table 1, sample 14).

### 3.4. Darkly Colored Surface Area

It is known that bulk ceramic materials are typically non-magnetic and non-conducting. However, in recent years, researchers have discovered that nanostructured materials possess unique properties compared to their bulk counterparts, owing to various defects that can influence their physical characteristics. Notably, unexpected magnetism has been observed in dielectric oxide nanostructured materials [35,36,53]. Numerous studies on magnetic oxides and nitrides have demonstrated that their magnetism can be attributed to the structural inhomogeneity of nanopowders and the presence of various defects in their structure, such as cationic and oxygen vacancies [36]. Additionally, magnetic titanium dioxide ( $\text{TiO}_2$ ) nanotubes have gained significant attention recently due to their potential applications in spintronics, where both charge and spin are employed in  $\text{TiO}_2$  nanotubes and nanorods [53].

As per our previous research, certain ceramic composite materials based on plasma-chemical powders displayed a distinct darkly colored region in the outer volume of the samples, aligned parallel to the direction of hot pressing (Figure 7). The most distinct dark area was observed in samples based on SIALON with 40 wt. % TiN. Interestingly, by increasing the dwell time from 1 to 8 min during the hot-pressing process, the thickness of this dark area increased or completely disappeared. Surprisingly, no significant differences in the physico-mechanical properties (wear, hardness, and fracture toughness) were found between the different colored areas of the samples under the given study conditions. Despite the visual appearance of the dark areas, they did not seem to have a notable impact on the material's performance.



**Figure 7.** Thickness of the dark area of ceramic composite materials based on plasma-chemical powders based on  $\text{Si}_3\text{N}_4$ ,  $\text{Si}_3\text{N}_4\text{—TiN}$ , SIALON—TiN vs. dwell time of hot pressing: (a)—1 min, (b)—8 min.

The appearance of a skin layer near the surface of hot-pressed silicon nitride ceramics, exhibiting a different color tone from the bulk body, was also observed in [33]. However, the explanation provided in [33] regarding the increase in the thickness of the dark-colored area due to the increase in sintering additives from 6 wt.% to 8 wt.% seems less convincing. This is because the increase in sintering additives from 8 wt.% to 12 wt.% had much less impact on the thickness of the dark-colored area.

Additionally, the content of yttrium and magnesium, as revealed by the EDS analysis of the grain-boundary glassy phase, contradicts the findings presented in Figure 7, where ceramics without yttrium and magnesium based on SIALON-TiN still displayed coloration. Moreover, the differences observed in the electron images of the skin layer and the bulk of hot-pressed silicon nitride ceramics were negligible and within the margin of error. Furthermore, the X-ray diffraction patterns of the hot-pressed silicon nitride ceramics for both the skin layer and bulk area appeared the same [33]. Considering the observations and previous research findings, it is indeed more plausible that the coloration of the darkly colored regions in the ceramic composite materials is caused by the presence of  $\text{Si}_3\text{N}_4$ .

The magnetism observed in  $\text{Si}_3\text{N}_4$  plasma-chemical powders is attributed to structural inhomogeneity and the presence of various defects, including cationic and oxygen vacancies. Consequently, hot-pressed ceramic materials undergo changes in their optical properties when exposed to an electromagnetic field during induction heating.

An extended dwell time during induction heating of the nanopowder and an increase in sintering additives promote the alignment of a higher number of dipoles within the electromagnetic field. This results in a noticeable increase in the size of the darkly colored area within the outer volume of the samples, running parallel to the direction of hot-pressing.

#### 4. Conclusions

Ceramic materials based on plasma-chemical nanopowders, as prepared, have a modified porous layer on the surface. When subjected to additional surface grinding, this layer is removed, resulting in increased density, hardness, and the number of acoustic emis-

sion signals. The occurrence of acoustic emission signals may indicate a transgranular or intergranular fracture of the composite ceramic structure after the surface grinding process.

Surface porosity and higher carbon content lead to increased wear of ceramic materials based on SiALON-reinforced TiN before additional surface grinding. Incorporating  $Y_2O_3$  in the composition of ceramics based on  $Si_3N_4$ -reinforced TiN prevents carbon infiltration into the bulk of the material and mitigates the grinding effect.

The presence of darkly colored areas on the surface of ceramics based on  $Si_3N_4$  plasma chemical powders provides confirmation of the occurrence of non-thermal micro-wave effects from the induction furnace on these nanoparticles.

**Funding:** This research received no external funding.

**Institutional Review Board Statement:** Not applicable.

**Informed Consent Statement:** Not applicable.

**Data Availability Statement:** Data sharing not applicable now.

**Acknowledgments:** I acknowledge support G.G. Gnesin, I.I. Osipova, and V.O. Kovylyayev.

**Conflicts of Interest:** The author declares no conflict of interest.

## References

1. Nishimura, T.; Xu, X.; Kimoto, K.; Hirotsaki, N.; Tanaka, H. Fabrication of silicon nitride nanoceramics—Powder preparation and sintering: A review. *Sci. Technol. Adv. Mater.* **2007**, *8*, 635–643. [[CrossRef](#)]
2. Hu, F.; Xie, Z.P.; Zhang, J.; Hu, Z.L.; An, D. Promising high-thermal-conductivity substrate material for high-power electronic device: Silicon nitride ceramics. *Rare Met.* **2020**, *39*, 463–478. [[CrossRef](#)]
3. Klemm, H. Silicon Nitride for High-Temperature Applications. *J. Am. Ceram. Soc.* **2010**, *93*, 1501–1522. [[CrossRef](#)]
4. Bocanegra-Bernal, M.H.; Matovic, B. Mechanical properties of silicon nitride-based ceramics and its use in structural applications at high temperatures. *Mater. Sci. Eng. A* **2010**, *527*, 1314–1338. [[CrossRef](#)]
5. Krstic, Z.; Krstic, V.D. Silicon nitride: The engineering material of the future. *J. Mater. Sci.* **2012**, *47*, 535–552. [[CrossRef](#)]
6. Riley, F. Silicon nitride and related materials. *J. Am. Ceram. Soc.* **2000**, *83*, 245. [[CrossRef](#)]
7. Kim, T.H.; Lee, S.; Park, D.W. Synthesis of Silicon Nitride Nanoparticles by Upcycling Silicon Wafer Waste Using Thermal Plasma Jets. *Materials* **2022**, *15*, 8796. [[CrossRef](#)]
8. Liu, W.; Tong, W.; He, R.; Wu, H.; Wu, S. Effect of the  $Y_2O_3$  additive concentration on the properties of a silicon nitride ceramic substrate. *Ceram. Int.* **2016**, *42*, 18641–18647. [[CrossRef](#)]
9. Li, S.; Xie, Z.; Xue, W.; Luo, X.; An, L. Sintering of high-performance silicon nitride ceramics under vibratory pressure. *J. Am. Ceram. Soc.* **2015**, *98*, 698–701. [[CrossRef](#)]
10. Zhou, Y.; Hyuga, H.; Kusano, D.; Matsunaga, C.; Hirao, K. Effects of yttria and magnesia on densification and thermal conductivity of sintered reaction-bonded silicon nitrides. *J. Am. Ceram. Soc.* **2019**, *102*, 1579–1588. [[CrossRef](#)]
11. Hampshire, S. Silicon nitride Ceramics—review of structure, processing and properties. *J. Achiev. Mater. Manuf. Eng.* **2007**, *24*, 43.
12. Zhu, X.; Hayashi, H.; Zhou, Y.; Hirao, K. Influence of additive composition on thermal and mechanical properties of  $\beta$ - $Si_3N_4$  ceramics. *J. Mater. Res.* **2004**, *19*, 3270–3278. [[CrossRef](#)]
13. Matovic, B.; Rixecker, G.; Aldinger, F. Pressureless sintering of silicon nitride with lithia and yttria. *J. Eur. Ceram. Soc.* **2004**, *24*, 3395–3398. [[CrossRef](#)]
14. Kusano, D.; Hyuga, H.; Zhou, Y.; Hirao, K. Effect of Aluminum Content on Mechanical Properties and Thermal Conductivities of Sintered Reaction-Bonded Silicon Nitride. *Int. J. Appl. Ceram. Technol.* **2014**, *11*, 534–542. [[CrossRef](#)]
15. Zhang, Y.; Xiao, G.; Yi, M.; Xu, C. Effect of graphene orientation on microstructure and mechanical properties of silicon nitride ceramics. *Process. Appl. Ceram.* **2018**, *12*, 27–35. [[CrossRef](#)]
16. Šajgalik, P.; Dusza, J.; Hoffmann, M.J. Relationship between Microstructure, Toughening Mechanisms, and Fracture Toughness of Reinforced Silicon Nitride Ceramics. *J. Am. Ceram. Soc.* **1995**, *78*, 2619–2624. [[CrossRef](#)]
17. Pyzik, A.J.; Beaman, D.R. Microstructure and Properties of Self-Reinforced Silicon Nitride. *J. Am. Ceram. Soc.* **1993**, *76*, 2737–2744. [[CrossRef](#)]
18. Švec, P.; Brusilová, A.; Kozánková, J. Effect of microstructure and mechanical properties on wear resistance of silicon nitride ceramics. *Mater. Eng.* **2008**, *16*, 34–40.
19. Li, S.; Wei, C.; Zhou, L.; Wang, P.; Wang, W. Microstructure and fracture strength of silicon nitride ceramics consolidated by oscillatory pressure sintering. *Ceram. Int.* **2019**, *45*, 15671–15675. [[CrossRef](#)]
20. Iturriza, I.; Castro, F.; Fuentes, M. Sinter and sinter-HIP of silicon nitride ceramics with yttria and alumina additions. *J. Mater. Sci.* **1989**, *24*, 2047–2056. [[CrossRef](#)]
21. Guedes-Silva, C.C.; De Souza Carvalho, F.M.H.; Bressiani, J.C. Effect of rare-earth oxides on properties of silicon nitride obtained by normal sintering and sinter-HIP. *J. Rare Earths* **2012**, *30*, 1177–1183. [[CrossRef](#)]

22. Xu, W.; Yin, Z.; Yuan, J.; Wang, Z.; Fang, Y. Effects of sintering additives on mechanical properties and microstructure of Si<sub>3</sub>N<sub>4</sub> ceramics by microwave sintering. *Mater. Sci. Eng. A* **2017**, *684*, 127–134. [[CrossRef](#)]
23. Khajelakzay, M.; Bakhshi, S.R.; Borhani, G.H.; Ramazani, M. Synthesis and spark plasma sintering of the  $\alpha$ -Si<sub>3</sub>N<sub>4</sub> nanopowder. *Ceram. Int.* **2016**, *42*, 14867–14872. [[CrossRef](#)]
24. Golla, B.R.; Ko, J.W.; Kim, H.D. Processing and characterization of sintered reaction bonded Si<sub>3</sub>N<sub>4</sub> ceramics. *Int. J. Refract. Met. Hard Mater.* **2017**, *68*, 75–83. [[CrossRef](#)]
25. Han, Y.; Xie, Z.; Li, S.; Zhu, T.; Wu, W.; An, D.; Hu, F.; Zhai, F. Optimum sintering temperature of high quality silicon nitride ceramics under oscillatory pressure. *Ceram. Int.* **2018**, *44*, 6949–6952. [[CrossRef](#)]
26. Zhang, Y.W.; Yu, J.B.; Xia, Y.F.; Zuo, K.H.; Yao, D.X.; Zeng, Y.P.; Ren, Z.M. Microstructure and mechanical performance of silicon nitride ceramics with seeds addition. *J. Inorg. Mater.* **2012**, *27*, 807–812. [[CrossRef](#)]
27. Hirota, M.; Brito, M.E.; Hirao, K.; Watari, K.; Toriyama, M.; Nagaoka, T. Grain growth behavior during microwave annealing of silicon nitride. *Mater. Res. Soc. Symp. Proc.* **1996**, *430*, 441–445. [[CrossRef](#)]
28. Rutkowski, P.; Stobierski, L.; Górný, G. Thermal stability and conductivity of hot-pressed Si<sub>3</sub>N<sub>4</sub>-graphene composites. *J. Therm. Anal. Calorim.* **2014**, *116*, 321–328. [[CrossRef](#)]
29. Miranzo, P.; García, E.; Ramírez, C.; González-Julián, J.; Belmonte, M.; Osendi, M.I. Anisotropic thermal conductivity of silicon nitride ceramics containing carbon nanostructures. *J. Eur. Ceram. Soc.* **2012**, *32*, 1847–1854. [[CrossRef](#)]
30. Hirao, K.; Watari, K.; Brito, M.E.; Toriyama, M.; Kanzaki, S. High Thermal Conductivity in Silicon Nitride with Anisotropic Microstructure. *J. Am. Ceram. Soc.* **1996**, *79*, 2485–2488. [[CrossRef](#)]
31. Sun, E.Y.; Becher, P.F.; Plucknett, K.P.; Hsueh, C.; Alexander, K.B.; Waters, S.B. Microstructural Design of Silicon Nitride with Improved Fracture Toughness: II, Effects of Ytria and Alumina Additives. *J. Am. Ceram. Soc.* **1998**, *40*, 2821–2830. [[CrossRef](#)]
32. Yu, J.J.; Guo, W.M.; Wei, W.X.; Lin, H.T.; Wang, C.Y. *Fabrication and Wear Behaviors of Graded Si<sub>3</sub>N<sub>4</sub> Ceramics by the Combination of Two-Step Sintering and  $\beta$ -Si<sub>3</sub>N<sub>4</sub> Seeds*; Elsevier Ltd.: Amsterdam, The Netherlands, 2018; Volume 38, pp. 3457–3462.
33. Mishima, M.; Sato, Y.; Ueki, M. Relation between microstructure and color tone of skin layer and bulk area of silicon nitride ceramics. *Nippon. Seramikusu Kyokai Gakujutsu Ronbunshi J. Ceram. Soc. Jpn.* **1992**, *100*, 1323–1326. [[CrossRef](#)]
34. Terwilliger, G.R.; Lange, F.F. Pressureless sintering of Si<sub>3</sub>N<sub>4</sub>. *J. Mater. Sci.* **1975**, *10*, 1169. [[CrossRef](#)]
35. Chen, S.C.; Sung, K.Y.; Tzeng, W.Y.; Wu, K.H.; Juang, J.Y.; Uen, T.M.; Luo, C.W.; Lin, J.Y.; Kobayashi, T.; Kuo, H.C. Microstructure and magnetic properties of oxidized titanium nitride thin films in situ grown by pulsed laser deposition. *J. Phys. D Appl. Phys.* **2013**, *46*, 075002. [[CrossRef](#)]
36. Gong, C.; Meng, H.; Zhao, X.; Zhang, X.; Yu, L.; Zhang, J.; Zhang, Z. Unique Static Magnetic and Dynamic Electromagnetic Behaviors in Titanium Nitride/Carbon Composites Driven by Defect Engineering. *Sci. Rep.* **2016**, *6*, 18927. [[CrossRef](#)]
37. Millers, T.; Grabis, J.; Zálite, I. Ultrafine Powders of the Refractory Materials in the Composite Development BT. In Proceedings of the MICC 90: Moscow International Composites Conference, Moscow, Russia, 14–16 November 1990; Fridlyander, I.N., Kostikov, V.I., Eds.; Springer: Dordrecht, The Netherlands, 1991; pp. 151–153, ISBN 978-94-011-3676-1.
38. Zálite, I.; Herrmann, M.; Grabis, J. Materials on the Basis of Finely Dispersed Si<sub>3</sub>N<sub>4</sub> Powders. *Key Eng. Mater.* **1997**, *132–136*, 1018–1021. [[CrossRef](#)]
39. Osipova, I.I.; Sartinskaya, L.L. Effect of processing factors on the structural heterogeneity of materials based on ultrafine nitride powders. *Powder Metall. Met. Ceram.* **1990**, *29*, 7–9. [[CrossRef](#)]
40. Gnesin, G.G.; Osipova, I.I.; Sartinskaya, L.L.; Grigor'ev, O.N. Properties of materials based on ultradispersed nitride powders. *Powder Metall. Met. Ceram.* **1990**, *29*, 668–671. [[CrossRef](#)]
41. Gnesin, G.G.; Osipova, I.I.; Sartinskaya, L.L. Tool Ceramic Materials Based on Ultradispersed Nitride Powders. *Poroshkovaya Metall.* **1990**, *12*, 78–82.
42. Gnesin, G.G.; Osipova, I.I.; Sartinskaya, L.L. Ultradispersed nitride powder-base ceramic tool materials. *Powder Metall. Met. Ceram.* **1990**, *29*, 1011–1014. [[CrossRef](#)]
43. Niihara, K.; Morena, R.; Hasselman, D.P.H. Evaluation of K<sub>IC</sub> of brittle solids by the indentation method with low crack-to-indent ratios. *J. Mater. Sci. Lett.* **1982**, *1*, 13–16. [[CrossRef](#)]
44. Boyarskaya, Y.S.; Grabko, D.Z.; Katz, M.S. *Physics of Microindentation Processes*; Shtiintsa: Kichineu, Moldova, 1986.
45. Eitzen, D.G.; Wadley, H.N.G. Acoustic Emission: Establishing the Fundamentals. *J. Res. Natl. Bur. Stand.* **1984**, *89*, 75–100. [[CrossRef](#)] [[PubMed](#)]
46. Sakoman, M.; Ćorić, D.; Vuić, D. Load dependence of hardness and fracture toughness values on hardmetals. In *Abstracts Book and Proceedings on USB of International Conference on Materials, Tribology, Recycling, MATRIB 2016/Žmak, Irena; Aleksandrov Fabijanić, Tamara; Ćorić, Danko (ur.)*; Hrvatsko Društvo za Materijale i Tribologiju: Zagreb, Croatia, 2016; pp. 366–372.
47. Wang, P.; Kumar, R.; Sankaran, E.M.; Qi, X.; Zhang, X.; Popov, D.; Cornelius, A.L.; Li, B.; Zhao, Y.; Wang, L. Vanadium Diboride (VB<sub>2</sub>) Synthesized at High Pressure: Elastic, Mechanical, Electronic, and Magnetic Properties and Thermal Stability. *Inorg. Chem.* **2018**, *57*, 1096–1105. [[CrossRef](#)] [[PubMed](#)]
48. Osipova, I.I.; Sartinskaya, L.L.; Grigor'ev, O.N. Stabilization of properties of tool materials made of ultrafine powders. *Phys. Mater. Sci. Phys. Chem. Princ. Dev. New Mater.* **1989**, 129–133.
49. Osipova, I.I.; Koval'chenko, A.M.; Sartinskaya, L.L. Optimization of the composition of nitridic ceramic tool material by tribotechnical tests. *Powder Metall. Met. Ceram.* **1992**, *31*, 321–324. [[CrossRef](#)]

50. Osipova, I.I.; Kovalchenko, A.M.; Sartinskaya, L.L. Tribotechnical Tests of Tool Nitride Ceramics. *Poroshkovaya Metall.* **1992**, *4*, 46–51.
51. Osipova, I.I.; Koldaev, N.V.; Sartinskaya, L.L. Mechanical properties of materials of ultradispersed nitride and oxide powders. *Powder Metall. Met. Ceram.* **1996**, *34*, 573–578. [[CrossRef](#)]
52. Sartinska, L.L.; Gnesin, G.G.; Osipova, I.I. Ceramic composites based on  $\text{Si}_3\text{N}_4$ -TiN. In Proceedings of the CERAM-2001: International Conference on Advanced Ceramics for the Third Millenium, Tokyo, Japan, 6–8 September 2001; p. 2001.
53. Alivov, Y.; Grant, T.; Capan, C.; Iwamoto, W.; Pagliuso, P.G.; Molloy, S. Origin of magnetism in undoped  $\text{TiO}_2$  nanotubes. *Nanotechnology* **2013**, *24*, 275704. [[CrossRef](#)]

**Disclaimer/Publisher’s Note:** The statements, opinions and data contained in all publications are solely those of the individual author(s) and contributor(s) and not of MDPI and/or the editor(s). MDPI and/or the editor(s) disclaim responsibility for any injury to people or property resulting from any ideas, methods, instructions or products referred to in the content.